AGU ADVANCING EARTH AND SPACE SCIENCES

Geophysical Research Letters

RESEARCH LETTER
10.1029/2025GL119325

Frequency-Dependent Anisotropy and Upper Plate Deformation Due To Seamount Subduction in Northern Luzon

Lingmin Cao[1,2], Xiaobo He[3], Liang Zhao[4,5], Bor-Shouh Huang[6], Tianyao Hao[5,7], Minghui Zhao[2,5], Xuelin Qiu[2,5], Enyuan He[2], Kuiyuan Wan[2], Yunfan Zhang[2], and Huaiyu Yuan[8,9]

[1]Yazhou Bay Innovation Institute, College of Marine Science and Technology, Hainan Tropical Ocean University, Sanya, China, [2]State Key Laboratory of Tropical Oceanography, South China Sea Institute of Oceanology, Chinese Academy of Sciences, Guangzhou, China, [3]Department of Ocean Exploration and Technology, Zhejiang Ocean University, Zhoushan, China, [4]State Key Lab of Lithospheric Evolution, Institute of Geology and Geophysics, Chinese Academy of Sciences, Beijing, China, [5]University of Chinese Academy of Sciences, Beijing, China, [6]Institute of Earth Sciences, Academia Sinica, Taipei, Taiwan, [7]Key Lab of Petroleum Resources Research, Institute of Geology and Geophysics, Chinese Academy of Sciences, Beijing, China, [8]School of Natural Sciences, Macquarie University, Sydney, NSW, Australia, [9]Centre for Exploration Targeting, University of Western Australia, Perth, WA, Australia

Abstract Seamount subduction influences subduction zone dynamics by altering stress fields, fracture patterns, and seismic anisotropy. This study utilizes local *S*-wave splitting analysis to investigate crustal and upper mantle deformation associated with seamount subduction beneath northern Luzon. Our observations reveal predominantly trench-normal fast-axis orientations and frequency-dependent delay times. These patterns suggest that anisotropy arises primarily from fluid-filled cracks and possible serpentinization, with effects extending from the overriding crust into the subducting slab, spanning multiple structural depths. In contrast, trench-parallel directions in southern non-seamount subduction regions indicate either ductile overriding lithosphere deformation or toroidal mantle flow around the slab edge. Event depth and raypath geometry further indicate that seamount subduction promotes stress heterogeneity and vertical anisotropic layering. These findings demonstrate that subducting features such as seamounts produce distinct anisotropy signatures, offering new insights into subduction dynamics and lithospheric deformation.

Plain Language Summary Subduction zone dynamics are affected by geological features like seamounts. These features can change how stress is distributed, how fractures form, and how seismic waves travel through the Earth. In this study, we analyzed shear wave splitting to understand how seamount subduction impacts the crust and upper mantle deformation beneath northern Luzon. We found that fast directions are perpendicular to the trench, and the delay times depend on the frequency of the waves, which can be explained by fluid-filled cracks and possible serpentinization in the subducting slab. Interestingly, we observed distinct trench-parallel directions at non-seamount subduction areas. These results show that subducting seamounts leave unique seismic signatures, providing new insights into how subduction zones work and how the lithosphere deforms in response.

Key Points:

- Seamount subduction reshapes stress, fractures, and seismic anisotropy in northern Luzon's crust and upper mantle
- Trench-normal anisotropy in the north reflects seamount-slab interactions; trench-parallel in the south shows mantle flow
- Unique seismic patterns reveal how subducting features influence subduction dynamics and lithospheric deformation

Supporting Information:

Supporting Information may be found in the online version of this article.

Correspondence to:

L. Cao and X. He,
cao_lingmin@126.com;
xiaobo.he@zjou.edu.cn

Citation:

Cao, L., He, X., Zhao, L., Huang, B.-S., Hao, T., Zhao, M., et al. (2025). Frequency-dependent anisotropy and upper plate deformation due to seamount subduction in northern Luzon. *Geophysical Research Letters*, *52*, e2025GL119325. https://doi.org/10.1029/2025GL119325

Received 7 SEP 2025
Accepted 5 NOV 2025

Author Contributions:

Conceptualization: Xiaobo He
Data curation: Lingmin Cao, Enyuan He
Formal analysis: Lingmin Cao, Xiaobo He
Funding acquisition: Liang Zhao, Tianyao Hao
Investigation: Bor-Shouh Huang
Methodology: Xiaobo He
Resources: Bor-Shouh Huang
Supervision: Xiaobo He, Liang Zhao
Validation: Liang Zhao, Minghui Zhao, Xuelin Qiu, Enyuan He, Kuiyuan Wan
Visualization: Lingmin Cao, Tianyao Hao, Yunfan Zhang
Writing – original draft: Lingmin Cao

1. Introduction

The ocean seafloor exhibits significant topographic diversity, characterized by features such as mid-ocean ridges, seamounts, remnant arc ridges, and plateaus, collectively covering approximately 20%–30% of the ocean surface (Harris et al., 2014; Yesson et al., 2011). When these elevated seafloor structures subduct, they generate unique plate configurations, for example, the Peruvian flat slab (e.g., Dougherty & Clayton, 2014; Hasegawa & Sacks, 1981) and the Manila slab window (e.g., Bautista et al., 2001; Fan & Zhao, 2021). These configurations significantly affect the deformation of the overriding plate, the surrounding mantle, and the subducted slab itself (Baba et al., 2001; Cloos, 1992; Eakin et al., 2015, 2016; He & Zhou, 2024; Scholz & Small, 1997). Seamount subduction has been associated with the formation of fracture networks that facilitate aseismic creep and generate small earthquakes in the upper mantle (Tan et al., 2022; K. Wang & Bilek, 2011, 2014). However, further seismological evidence is required to validate these hypotheses.

Writing – review & editing: Xiaobo He, Liang Zhao, Huaiyu Yuan

One promising approach involves analyzing seismic anisotropy that may be influenced by the presence of fluids and associated deformation fabrics (e.g., Cao et al., 2019; Cao, He, et al., 2024; Hammond et al., 2010; Leidig & Zandt, 2003). In particular, frequency-dependent variations in shear wave splitting delay times can provide valuable constraints on the distribution and scale of anisotropic structures (e.g., Z. Huang et al., 2011), thereby offering insights into deformation processes and possible fracture systems in the overriding crust and upper mantle.

In this study, we focus on northern Luzon (Figure 1), where the South China Sea (SCS) plate, accompanied by seamounts, subducts beneath the region. Globally, local *S*-wave splitting measurements often reveal trench-parallel fast directions in the forearc regions. However, exceptions occur in subduction zones like South America, Alaska, Central America, and Southwestern Japan, where fast directions are trench-perpendicular, often due to subducted seamounts or ridges (Figure 1a, Celis et al., 2022; Long & Wirth, 2013; Lynner et al., 2024; Volti et al., 2005). Despite these observations, frequency-dependent anisotropy has not been systematically investigated in such regions.

Here, we aim to address this gap by examining the occurrence of frequency-dependent anisotropy in the northern Luzon subduction zone. By analyzing local shear wave splitting, we seek to provide new insights into upper-mantle deformation.

2. Tectonic Settings

At present, the SCS plate is subducting beneath northern Luzon along the Manila Trench, with convergence rates increasing from ∼52 mm/yr at ∼15°N to ∼98 mm/yr at ∼18°N (Figure 1a, Pautot & Rangin, 1989; Rangin et al., 1999; Tsai et al., 1981). Recent Bathymeter Sonar Systems surveys reveal that the Zhenbei-Huangyan seamount chain (also known as the Scarborough seamount chain) and the fossil ridge of the SCS are currently being subducted together at their intersection with the Manila Trench near ∼16°N (Figure 1a, Li et al., 2004; Pautot & Rangin, 1989).

The subduction of the fossil ridge and seamounts exerts significant effects on subduction zone dynamics (e.g., DeLong et al., 1979; Iwamori, 2000; Lallemand et al., 1992). Regional and global tomographic studies (e.g., Fan & Zhao, 2021; Koulakov et al., 2014; Lallemand et al., 2001; Z. Wang et al., 2006; Zhao et al., 2013) have revealed the geometry of the subducting SCS slab, which has been influenced by the subduction of the ridge and seamounts, and indicated that the dip angles of the Manila slab vary along the Manila Trench: approximately 25° between 18°N and 21°N, increasing to 32°N at 17°N, and becoming nearly vertical at 14°N. The subduction of the SCS ridge may play a role in creating slab tearing as it subducts beneath Luzon Island (Fan & Zhao, 2021; Fan et al., 2015), influencing arc volcanism (Yang et al., 1996). These characteristics make northern Luzon Island an ideal area to investigate crustal and upper mantle deformation associated with the subduction of bathymetric features.

3. Data and Analysis

We used six broadband stations from the Institute of Earth Sciences of Academia Sinica, Taipei, deployed on Luzon Island in collaboration with the Philippine Institute of Volcanology and Seismology (PHIVOLCS), Philippines, starting in 2010 (Figure 1 and Table S1 in Supporting Information S1). We analyzed *S*-wave waveforms from local earthquakes recorded at each station within the Manila subduction zone. Events from 2010 to 2016 with magnitudes greater than 3.0 were selected from the International Seismic Center Engdahl-van der Hilst-Buland (ISC-EHB) catalog (Engdahl et al., 2020).

We manually inspected all waveforms to measure local *S*-phase splitting and selected only those with a signal-to-noise ratio (SNR) greater than 3. Seismograms were chosen for events at each station within a 35° cone of incident angle (i.e., the so-called "shear wave window"; Booth & Crampin, 1985) to avoid waveform contamination by s-to-p conversions in the crustal interfaces. Original broadband waveforms were band-pass filtered using both high-frequency (1–4 Hz) and low-frequency (0.1–1 Hz) bands, similar to the filters used in Audoine et al. (2004) for local *S* splitting measurements.

Shear wave splitting analyses for each eligible event-station pair were conducted using the widely used MFAST program (Savage et al., 2010; Teanby et al., 2004), which has been extensively applied in subduction zone studies (e.g., Hammond et al., 2010; Kong et al., 2020; Liu et al., 2008). MFAST implements the minimum eigenvalue

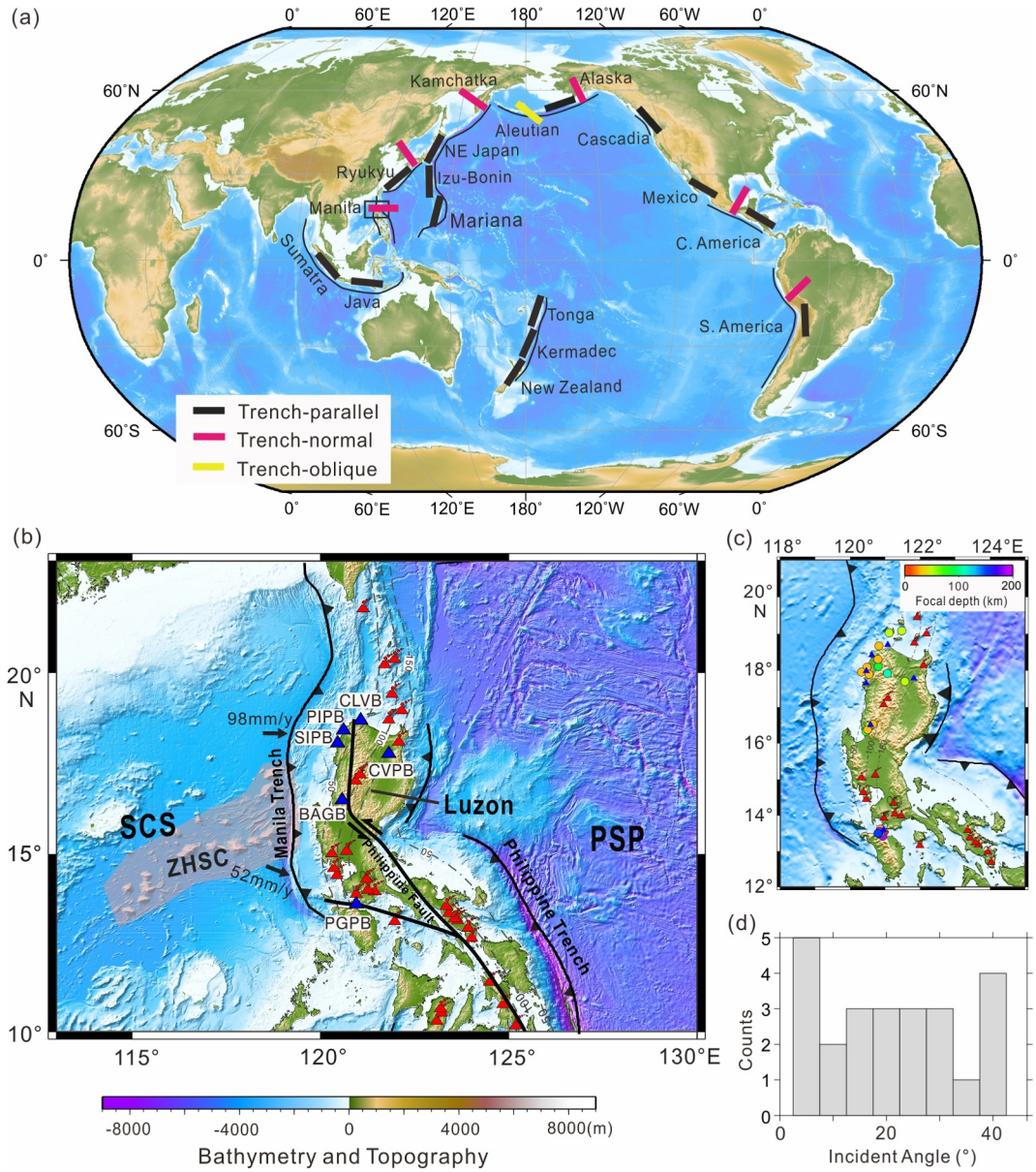

Figure 1. (a) Summary map of forearc lithosphere deformation worldwide compiled from local *S*-wave splitting measurements from Volti et al. (2005), Long and Wirth (2013), Eakin et al., 2015, 2016, Celis et al. (2022), and Lynner et al. (2024). Fast polarization directions are trench-parallel in most subduction zones, except Southern America, Alaska, Central America, Southwestern Japan, and Manila (our study area shown within black rectangle). (b) Tectonic settings of the Luzon Island and station locations (blue triangles). Solid red triangles indicate Quaternary volcanoes. Black arrows represent the convergence rates along the trench (Pautot & Rangin, 1989; Rangin et al., 1999; Tsai et al., 1981). PSP, Philippine Sea Plate; SCS, South China Sea; and ZHSC, Zhenbei-Huangyan seamount chain (translucent shaded region). The gray dot-dash contour lines show projected depths of the upper boundaries of the subducting South China Sea slab with an interval of 50 km from Slab2 (Hayes et al., 2018). (c) Local events used in the final splitting analysis are shown as circles, colored according to the event depth. (d) Histograms of incident angles for all local *S* phases used in the final splitting analysis with a frequency bandfilter between 1 and 4 Hz.

method of Silver and Chan (1991). In this study, we applied the standard MFAST package following the workflow of Cao, He, et al. (2024) and Cao, Lü, et al. (2024), proven effective for local *S*-wave splitting in subduction settings including the North Sulawesi and Hikurangi subduction zones (Cao, He, et al., 2024; Cao, Lü, et al., 2024; Castellazzi et al., 2015). To minimize potential cycle-skipping effects, analysis windows spanned at least one full *S*-wave period and were chosen based on waveform clarity and theoretical arrival times, carefully

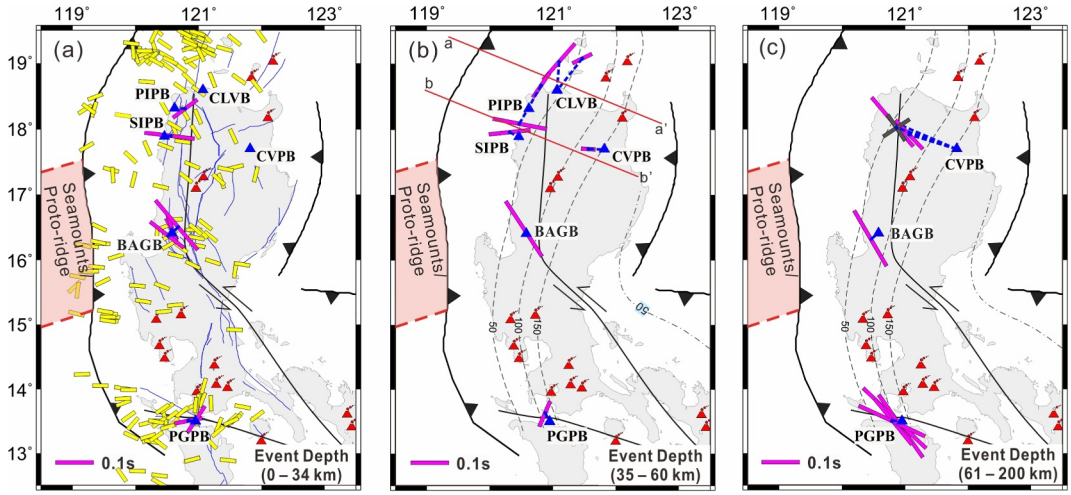

Figure 2. Results at all six stations measured in the high-frequency band (1–4 Hz) with focal depths between 0 and 35 km, between 35 and 60 km, and between 60 and 200 km are plotted, respectively. Yellow bars in panel (a) denote the P-axes projected to the surface for the well-determined focal mechanisms of events shallower than 35 km from the Global CMT catalog. Dashed contour lines in panels (b, c) show projected depths of the upper boundaries of the subducting South China Sea and Philippine Sea slabs, with an interval of 50 km, based on the Slab2 model (Hayes et al., 2018). Pink bars show the fast polarization directions, with lengths proportional to the measured delay times, and are plotted at the earthquake epicenters. Blue triangles represent stations. Earthquakes located near the two red solid lines in panel (b) are projected onto the along-profile cross sections shown in Figure S4 in Supporting Information S1. A dark gray cross in panel (c) represents a null measurement, indicating the components of incoming polarization direction and its perpendicular.

avoiding contamination from later phases. MFAST then performs a grid search over possible φ (fast direction) and δt (delay time) values to determine the optimal splitting parameters and derives the initial polarization direction from the particle motion, making it well suited for local *S*-wave studies. Reported measurement uncertainties correspond to one standard deviation (Marson-Pidgeon & Savage, 2004).

More specifically, anisotropy measurements are considered well-constrained when they satisfy the following criteria: (a) a strong correlation between the fast and slow waveforms, (b) minimal amplitude on the component perpendicular to the incoming polarization direction of local *S*, (c) clear linearization of particle motion after correction, and (d) a small 95% confidence region. Each measurement is derived from a single carefully selected window, as illustrated in Figure S1 in Supporting Information S1. Note that null results can occur when the shear wave travels through an isotropic medium or when the initial polarization aligns with either the fast or slow polarization direction. In such cases, no *S*-wave energy appears on the component perpendicular to the incoming polarization, and the particle motion remains linear. An example of a null measurement is shown in Figure S2 in Supporting Information S1. Applying these quality control criteria, we obtained 24 and 10 well-constrained splitting measurements for the high-frequency and low-frequency filters, respectively, along with one null measurement for the high-frequency filter (Figure 2, Figure S3 and Tables S2–S4 in Supporting Information S1).

4. Results

The Crust1.0 model indicates that Luzon's Moho depth is less than 33 km (Laske et al., 2012, 2013). Using this model as a reference, we classified the events into shallow earthquakes within the overlying crust (<35 km), intermediate-depth earthquakes (35–60 km) and deep earthquakes (>60 km) to illustrate the spatial and depth distribution in our results.

For shallow events at high-frequency band (Figure 2), *S*-wave splitting results show a clockwise rotation of fast direction, shifting from NE-SW at PIPB (oblique to the trench) to E-W at SIPB (normal to the trench) and SE-NW at BAGB (oblique to the trench) from north to center Luzon (Figure 2a). At the southernmost station, PGPB, the fast directions are trench-normal (Figure 2a). To facilitate comparison with regional stress status, we estimated the orientations of P-axes derived from moment tensor solutions of crustal earthquakes (Aki & Richards, 1980; He & Zhou, 2024). These P-axes were used to assess the relationship between maximum compressive stress

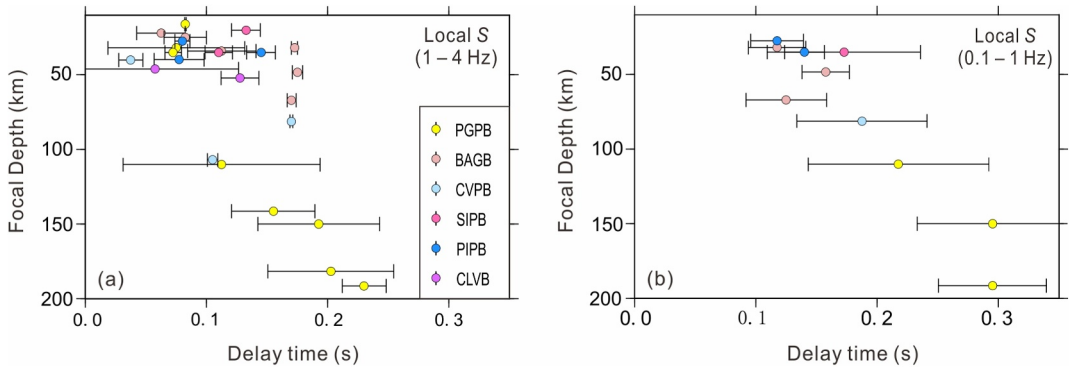

Figure 3. Focal depth versus delay times for events with the high (1–4 Hz) and low (0.1–1 Hz) frequency bandfilters across six stations.

directions and observed fast polarization directions. The detailed calculation procedure is described in Text S1 in Supporting Information S1. Fast directions at SIPB and PGPB align well with the P-axes, while others do not. The average δt for shallow events is moderate, with a mean of 0.10 ± 0.03 s, showing no apparent variation with focal depths (Figure 3a).

For intermediate-depth events (35–60 km), the fast directions are generally consistent with those at shallow depths (Figure 2b), with an average δt of 0.10 ± 0.04 s. At greater depths (>60 km), however, the fast directions exhibit more distinct patterns: predominantly NW-SE overall, but trench-normal at CVPB, oblique to the trench at BAGB, and trench-parallel at PGPB (Figure 2c). These deeper events also yield a larger mean δt of 0.17 ± 0.04 s. Notably, CVPB records the only null result in our data set, corresponding to an incoming *S*-wave polarization (−33.6°), which aligns well with the station's dominant fast direction.

In the low-frequency band, fast directions display more coherent spatial patterns than those observed at high frequencies. δt in this band range varies from 0.1 to 0.3 s (Figure 3 and Figure S3 in Supporting Information S1) with an average of 0.17 ± 0.07 s, higher than the mean of 0.12 ± 0.05 s observed in the high-frequency band. We also note low-frequency measurements yield higher δt at SIPB and PGPB but lower δt at BAGB than high-frequency measurements (Figure 3). For clarity, the following discussion primarily focuses on the high-frequency measurements unless stated otherwise.

5. Discussion

Seismic anisotropy provides key insights into deformation processes within the Earth. It is often interpreted as resulting from strain-induced crystallographic preferred orientation (CPO) in upper mantle mineral fabrics (e.g., Long & Silver, 2009; Savage, 1999). In subduction zones, two key processes induce CPO: two-dimensional corner flow, with fast directions usually perpendicular to the trench (Hanna & Long, 2012; Long & Silver, 2008, 2009; Lynner & Long, 2013; Russo & Silver, 1994), and toroidal flow around the slab edge, relevant when measurements are near the subducting slab edge (e.g., Cao et al., 2021; L. Wang & He, 2020). Another interpretation involves shape-preferred orientation, which can arise from sub-parallel structures like aligned cracks filled with fluids (e.g., Hammond et al., 2010; Leidig & Zandt, 2003). We will employ the two mechanisms and related dynamic processes to explain our measurements.

5.1. Frequency-Dependent Anisotropy

Finite-frequency theory suggests that the first Fresnel zone, where sensitivity to anisotropic structure is highest, expands as frequency decreases (Alsina & Snieder, 1995; Favier & Chevrot, 2003). Consequently, lower-frequency waves sample broader spatial scales, effectively smoothing out small-scale heterogeneities, while higher-frequency waves are more sensitive to fine-scale structural variations. Frequency-dependent anisotropy has been documented in several regions, including New Zealand (Greve et al., 2008; Marson-Pidgeon & Savage, 1997), Japan (Wirth & Long, 2010), the Marianas (Fouch & Fischer, 1998), and Australia (Clitheroe & Van Der Hilst, 1998). Results from frequency-dependent splitting highlight the structural complexity beneath subduction zones (Silver & Savage, 1994).

In this study, we examine frequency-dependent anisotropy in this region (Figure 3). Notably, the lower frequency band exhibits larger delay times (δt) compared to the higher frequency band (Figure 3), consistent with previous studies (e.g., Baird et al., 2013; Guo et al., 2022). These findings suggest that anisotropy is vertically heterogeneous and distributed across multiple layers within both the overriding plate and the subducting slab. This includes anisotropic zones in the shallow crust and upper mantle of the overriding plate, as well as deeper structures within the subducting slab. In the eastern SCS, anomalously elevated Vp/Vs ratios in the crust and upper mantle (Jiang et al., 2025) have been interpreted as evidence of hydration and serpentinization via seawater infiltration along crustal faults within the incoming oceanic plate, producing potentially anisotropic zones at various depths. Within this geological context—where pervasive fracturing and hydration are expected in both the upper plate and the incoming lithosphere—lower-frequency *S*-waves, which sample larger volumes, are more sensitive to vertically distributed anisotropic zones, resulting in larger δt values. This frequency dependence thus reflects vertical heterogeneity arising from widespread fracturing, hydration, and deformation across the subduction system.

5.2. Shear Deformation Near the Strike-Slip Philippine Fault

The Philippine Fault (PF) is a major strike-slip fault in this region, greatly influencing the regional crustal deformation. BAGB happens to be located near this fault, providing insights into the fault-related deformation. At BAGB, δt from two events at 22 and 25 km depths are 0.06 and 0.08 s, respectively (Figure 2a and Table S2 in Supporting Information S1). Both events exhibit consistent NW–SE-trending fast directions (Figure 2a). As estimated from P-axes near BAGB, the compressive stress direction is oriented E–W, perpendicular to the trench. P-axes pattern derived from earthquake focal mechanisms often aligns with principal stress directions when the axes are nearly horizontal. In our observations, however, fast directions at BAGB do not align with P-axes, implying that crust anisotropy beneath BAGB is not due to stress-induced crack alignment influenced by the tectonic stress (Crampin, 1994). Instead, these fast directions align with the strike of the PF, reflecting structure-induced anisotropy (Savage, 1999). Therefore, the PF plays a critical role in influencing the upper plate deformation.

5.3. Slab Edge Effect on the Mantle Flow at the Southern Margin

At the southernmost station, PGPB, three shallow earthquakes at depths of 16, 32, and 35 km reveal a prominent feature: fast directions predominantly parallel to the P-axes (Figures 2a and 2b), likely influenced by the maximum compressive stress field induced by the slab subduction. In contrast, for earthquakes at depths of 110–191 km (Figure 2c), fast-wave directions align with the strike of the subducting slab. We interpret these patterns as indicative of deformation linked to mantle flow around the slab edge, given that PGPB is situated at the boundary of the subducting SCS slab (Figure 4). Additionally, the larger δt values observed in the low-frequency results from deep earthquakes suggest that strong anisotropy arises from the upper mantle (Figure 3).

5.4. Seamount Subduction-Induced Trench-Normal Anisotropy

Events with raypaths beneath SIPB and to the south of PIPB intersect the segment of the slab influenced by the extinct spreading ridge and seamounts, yielding pronounced trench-normal fast directions from shallow to intermediate depths (Figures 2a and 2b). These fast directions align with P-axis orientations (Figure 2a), suggesting that stress-induced, fluid-rich fractures contribute to the observed anisotropy. Given focal depths of up to 35 km (Figure S4b in Supporting Information S1), such fractures likely exist in both the overriding plate and the subducting seamounts. Notably, our frequency-dependent measurements reveal that average δt (0.16 s) of two deeper events (35 km) in the low-frequency band is greater than that (0.13 s) of the high-frequency band (Tables S2 and S3 in Supporting Information S1). This frequency dependence indicates the presence of vertically distributed anisotropic layers, consistent with contributions from both the overriding plate and the subducting seamounts.

High-resolution bathymetric data from the East Caroline and Juan Fernández Ridges indicate that fractures and faults developed along seamount chains parallel to their strike (He et al., 2022). We attribute the trench-normal anisotropy in the subducting plate to seamount subduction, consistent with findings in Alaska, Central America, and Japan (Celis et al., 2022; Eakin et al., 2015; Volti et al., 2005). SIPB and PIPB are located near the northern boundary of the subducting seamount chains and the extinct spreading ridge, as indicated by the bathymetric highs. The earthquakes analyzed beneath these stations occurred directly below the stations, within the region affected by

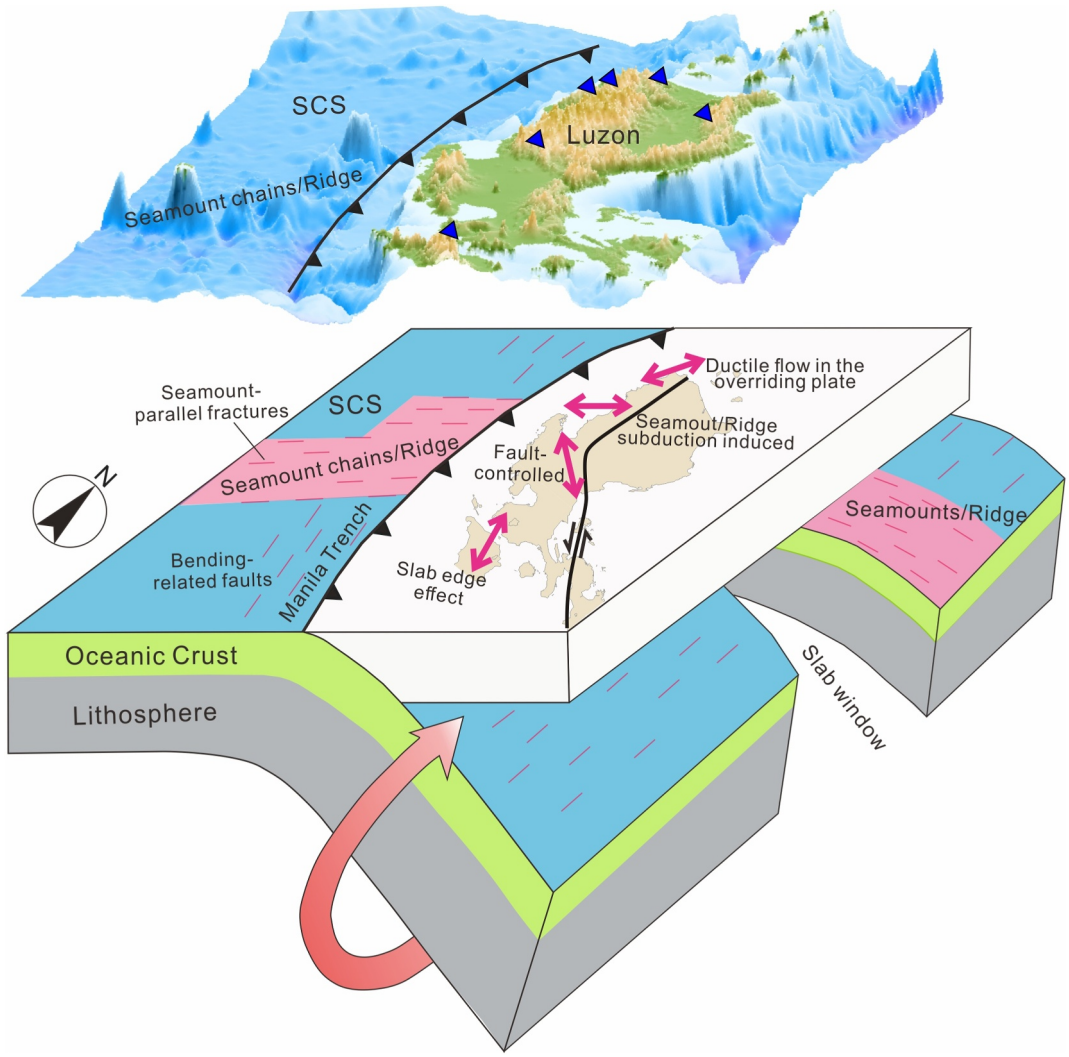

Figure 4. Schematic illustration of the tectonic setting with seamount and proto-ridge subduction in the Manila subduction zone and interpreted crustal deformation in the overlying and subducting plates, as well as in the upper mantle. The red arrow indicates mantle flow around the slab edge. The orientation of each double-headed arrow indicates the fast polarization direction observed at the station. SCS, South China Sea.

seamount subduction. This process likely reorients stress and induces trench-normal fracturing, supported by evidence that subducting seamounts promote fracturing and fluid ingress (Chesley et al., 2021; K. Wang & Bilek, 2011). Such hydration can lead to serpentinization under suitable conditions (Christensen, 2004), contributing to mineral-alignment anisotropy with trench-normal fast directions. Overall, stress-controlled fracturing appears to dominate anisotropy in the overriding crust, whereas serpentinization—particularly that associated with outer-rise faulting or seamount subduction—may contribute to anisotropy within the downgoing slab.

Recent studies from Japan provided independent support for our interpretation of seamount-induced anisotropy. Nakajima (2025) demonstrated that subducted seamounts can retain their structural integrity at depths exceeding 70 km, facilitating localized interplate earthquake clusters. Y. Huang et al. (2025) further showed that these earthquakes are associated with spatially confined anisotropic zones, likely reflecting damage and fluid infiltration. These findings supported our hypothesis that seamount subduction introduces stress heterogeneities and promotes trench-normal anisotropy within the slab. This aligned with previous evidence that seamount subduction alters slab structure, enhances localized hydration, and increases coupling variability—potentially reducing the likelihood of large megathrust earthquakes (Chesley et al., 2021; K. Wang & Bilek, 2011), favoring slow-slip and smaller earthquakes over major ruptures (Tan et al., 2022; K. Wang & Bilek, 2011, 2014).

5.5. Deformation in the Overriding Plate at the Northmost Luzon

At the northernmost station, CLVB, the observed splitting exhibits prominent trench-parallel fast directions nearly perpendicular to the P-axis orientations (Figure 2b). The two analyzed events beneath this station occurred at depths of 46 and 52 km and originate from the northeast, outside the region influenced by seamount subduction. In contrast, at PIPB, three events with ray paths from the east, northeast, and southwest show distinct splitting patterns. The southwest event, whose raypath intersects the subducted ridge and seamounts, displays a trench-normal fast direction, whereas the other two, located beyond the seamount-influenced zone, exhibit trench-parallel orientations (Figure 2a). This south-to-north transition from trench-normal to trench-parallel fast directions highlights the contrasting deformation regimes between seamount-influenced and non-seamount regions. The anisotropy in the latter, characterized by fast directions normal to the P-axes, likely reflects ductile deformation in the upper crust and lithospheric mantle rather than stress-induced, fluid-rich fracturing—a mechanism commonly invoked to explain the global trench-parallel azimuthal anisotropy in forearc areas (e.g., J. Wang et al., 2019).

Additionally, since two analyzed events are located within the subducting slab (Figure S4a in Supporting Information S1), part of the observed anisotropy may originate from a thin, hydrated anisotropic layer. In the offshore region, trench-parallel fast directions observed likely reflect anisotropy associated with serpentinization due to outer-rise faulting. This mechanism, involving fluid-filled cracks and aligned serpentine minerals, has been proposed as a source of slab anisotropy in several subduction zones (Healy et al., 2009). Similar trench-parallel splitting has been observed in Alaska and Japan, where it is attributed to strongly anisotropic serpentine minerals formed along bending-related outer-rise faults (Lynner, 2021; Wirth & Long, 2012).

5.6. 2-D Corner Flow Beneath the Arc Area

The station CVPB in the backarc region recorded shear-wave splitting from three earthquakes at depths of 40, 81, and 107 km. These events exhibit consistent fast directions perpendicular to the trench strike (Figures 2b and 2c). The 40-km earthquake has an E–W fast direction, aligning with the regional maximum compressive stress direction (Wu et al., 2017), potentially reflecting crustal anisotropy influenced by this stress field. For the two deeper events, fast polarization directions are oriented NW–SE, which are also consistent with predictions of our null measurement. Their ray paths, both originating from the NWW azimuth relative to CVPB, traverse the subducting slab, mantle wedge, lithospheric mantle, and overlying crust. The deeper events have longer delay times than the shallow events, suggesting that the NW-trending fast directions may indicate mineral CPO within the mantle wedge and/or lithospheric mantle, in line with widespread 2-D corner flow observed in other subduction zones (Long & Silver, 2008, 2009). In subduction zones, olivine fabrics are a key source of seismic anisotropy in the lithospheric mantle and mantle wedge. C- and E-type olivine fabrics typically develop at depths of ~60–150 km in the warm, hydrated portions of the mantle wedge, where slab-derived fluids promote hydrous slip systems and yield fast directions consistent with plate-motion directions (Jung & Karato, 2001; Karato et al., 2008; Katayama et al., 2004). The trench-normal fast directions observed at CVPB align with predictions for hydrous olivine CPO in the mantle wedge, where corner flow and slab-derived fluids influence deformation. Either C- or E-type fabrics likely dominate under the warm, hydrated conditions of the Manila subduction wedge, explaining the observed polarization pattern.

6. Conclusions

This study investigates the impact of seamount subduction on crustal and upper mantle deformation in the Manila subduction zone through local *S*-wave splitting analysis. Our findings, characterized by trench-normal fast-axis orientations and frequency-dependent delay times, provide critical insights into the deformation dynamics of northern Luzon:

1. Seamount Subduction and Trench-Normal Anisotropy: Trench-normal fast directions reflect stress reorientation and fracture alignment induced by seamount and ridge subduction. These features likely enhance fluid infiltration and localized hydration within the slab, promoting serpentinization and the development of anisotropic minerals aligned with trench-normal stresses. Such patterns are consistent with global observations in other subduction systems influenced by subducting bathymetric highs.
2. Frequency-Dependent Anisotropy: The frequency-dependent variations in delay times indicate vertically distributed and heterogeneous anisotropy. Such complexity may result from a combination of layered olivine

fabrics in the mantle, deformation within the overriding crust, and hydration- and/or serpentinization-related anisotropic structures in the subducting slab.

3. Regional Variation in Deformation: A northward transition from trench-normal to trench-parallel anisotropy reveal a dynamic interplay of ductile flow, faulting, and hydration processes. In contrast, trench-parallel anisotropy observed in the southern region suggest toroidal mantle flow around the slab edge.

Our results demonstrate how subduction of paleo-oceanic features, such as seamounts and ridges, generates distinctive seismic anisotropy signatures. These findings are consistent with global observations and underscore the significant role of subducting features in shaping the deformation and structural characteristics of subduction zones. By integrating constraints from frequency dependence and regional variations, this study highlights the combined contributions of the overriding plate, the subducting slab, and the mantle wedge to seismic anisotropy, providing a more balanced and physically grounded view of subduction dynamics.

Conflict of Interest

The authors declare no conflicts of interest relevant to this study.

Data Availability Statement

The list of shear wave splitting measurements is presented in Tables S2, S3 and S4 in Supporting Information S1. All the waveforms in the three components and results used in this study are available in Zenodo via L. Cao (2025). The shear waves splitting analysis software package used in this study—MFAST (Teanby et al., 2004) can be obtained via http://xn--mfastpackage-k09f.geo.vuw.ac.nz. Some figures were prepared using the Generic Mapping Tools (Wessel & Smith, 1991).

Acknowledgments
We want to express our sincere gratitude to Xiang Gao and Jianke Fan for their insightful comments and suggestions, which have significantly improved the quality of this manuscript. This research was supported by the National Scientific Foundation of China (Grants 42488201, 41888101, and 42366001) and the Development Fund of South China Sea Institute of Oceanology of Chinese Academy of Sciences (SCSIO202207).

References

Aki, K., & Richards, P. G. (1980). *Quantitative seismology, theory and methods* (Vol. 1). W. H. Freeman and Company.

Alsina, D., & Snieder, R. (1995). Small-scale sublithospheric continental mantle deformation: Constraints from SKS splitting observations. *Geophysical Journal International*, *123*(2), 431–448. https://doi.org/10.1111/j.1365-246x.1995.tb06864.x

Audoine, E., Savage, M. K., & Gledhill, K. (2004). Anisotropic structure under a back arc spreading region, the Taupo Volcanic Zone, New Zealand. *Journal of Geophysical Research*, *109*(B11), B11305. https://doi.org/10.1029/2003jb002932

Baba, T., Hori, T., Hirano, S., Cummins, P. R., Park, J. O., Kameyama, M., & Kaneda, Y. (2001). Deformation of a seamount subducting beneath an accretionary prism: Constraints from numerical simulation. *Geophysical Research Letters*, *28*(9), 1827–1830. https://doi.org/10.1029/2000gl012266

Baird, A. F., Kendall, J.-M., & Angus, D. A. (2013). Frequency-dependent seismic anisotropy due to fractures: Fluid flow versus scattering. *Geophysics*, *78*(2), WA111–WA122. https://doi.org/10.1190/geo2012-0288.1

Bautista, B. C., Bautista, M. L. P., Oike, K., Wu, F. T., & Punongbayan, R. S. (2001). A new insight on the geometry of subducting slabs in northern Luzon, Philippines. *Tectonophysics*, *339*(3–4), 279–310. https://doi.org/10.1016/s0040-1951(01)00120-2

Booth, D. C., & Crampin, S. (1985). Shear-wave polarization on a curved wavefront at an isotropic free surface. *Geophysical Journal of the Royal Astronomical Society*, *83*(1), 31–45. https://doi.org/10.1111/j.1365-246x.1985.tb05154.x

Cao, L. M. (2025). Local S recorded by stations in North Luzon. https://doi.org/10.5281/zenodo.14664573

Cao, L. M., He, X. B., Yuan, H. Y., Zhao, M. H., Qiu, X. L., & Savage, M. (2024). Upper-mantle seismic anisotropy in the southwestern North Island, New Zealand: Implications for regional upper-mantle and slab deformation. *Tectonophysics*, *887*, 230455. https://doi.org/10.1016/j.tecto.2024.230455

Cao, L. M., He, X. B., Zhao, L., Lü, C., Hao, T. Y., Zhao, M. H., & Qiu, X. L. (2021). Mantle flow patterns beneath the junction of multiple subduction systems between the Pacific and Tethys domains, SE Asia: Constraints from SKS-wave splitting measurements. *Geochemistry, Geophysics, Geosystems*, *22*(9), e2021GC009700. https://doi.org/10.1029/2021GC009700

Cao, L. M., Kao, H., Wang, K. L., Chen, C. X., Mori, L., Ohmi, S., & Gao, Y. (2019). Spatiotemporal variation of crustal anisotropy in the source area of the 2004 Niigata, Japan earthquake. *Bulletin of the Seismological Society of America*, *109*(4), 1331–1342. https://doi.org/10.1785/0120180195

Cao, L. M., Lü, C. C., He, X. B., Rawlinson, N., Hao, T. Y., Widiyantoro, S., et al. (2024). Mantle flow induced by the interplay of downgoing slabs revealed by seismic anisotropy beneath the Sula block in eastern Indonesia. *Journal of Geophysical Research: Solid Earth*, *129*(5), e2023JB028110. https://doi.org/10.1029/2023JB028110

Castellazzi, C., Savage, M. K., Walsh, E., & Arnold, R. (2015). Shear wave automatic picking and splitting measurements at Ruapehu volcano, New Zealand. *Journal of Geophysical Research: Solid Earth*, *120*(5), 3363–3384. https://doi.org/10.1002/2014jb011585

Celis, S., Valenzuela, R. W., Soto, G. L., & Pérez-Campos, X. (2022). Upper mantle and continental crust anisotropy in southeastern Mexico determined from shear-wave splitting measurements using local intraslab earthquakes. *Journal of South American Earth Sciences*, *119*, 104023. https://doi.org/10.1016/j.jsames.2022.104023

Chesley, C., Naif, S., Key, K., & Bassett, D. (2021). Fluid-rich subducting topography generates anomalous forearc porosity. *Nature*, *595*(7866), 255–260. https://doi.org/10.1038/s41586-021-03619-8

Christensen, N. I. (2004). Serpentinites, peridotites, and seismology. *International Geology Review*, *46*(9), 795–816. https://doi.org/10.2747/0020-6814.46.9.795

Clitheroe, G., & Van Der Hilst, R. D. (1998). Complex anisotropy in the Australian lithosphere from shear-wave splitting in broad-band SKS records. *Structure and Evolution of the Australian Continent*, *26*, 73–78. https://doi.org/10.1029/gd026p0073

Cloos, M. (1992). Thrust-type subduction-zone earth quakes and seamount asperities: A physical model for seismic rupture. *Geology*, *20*(7), 601–604. https://doi.org/10.1130/0091-7613(1992)020<0601:ttszea>2.3.co;2

Crampin, S. (1994). The fracture criticality of crustal rocks. *Geophysical Journal International*, *118*(2), 428–438. https://doi.org/10.1111/j.1365-246x.1994.tb03974.x

DeLong, S. E., Schwarz, W. M., & Anderson, R. N. (1979). Thermal effects of ridge subduction. *Earth and Planetary Science Letters*, *44*(2), 239–246. https://doi.org/10.1016/0012-821x(79)90172-9

Dougherty, S. L., & Clayton, R. W. (2014). Seismic structure in southern Peru: Evidence for a smooth contortion between flat and normal subduction of the Nazca plate. *Geophysical Journal International*, *200*(1), 534–555. https://doi.org/10.1093/gji/ggu415

Eakin, C. M., Long, M. D., Scire, A., Beck, S. L., Wagner, L. S., Zandt, G., & Tavera, H. (2016). Internal deformation of the subducted Nazca slab inferred from seismic anisotropy. *Nature Geoscience*, *9*(1), 56–59. https://doi.org/10.1038/ngeo2592

Eakin, C. M., Long, M. D., Wagner, L. S., Beck, S. L., & Tavera, H. (2015). Upper mantle anisotropy beneath Peru from SKS splitting: Constraints on flat slab dynamics and interaction with the Nazca Ridge. *Earth and Planetary Science Letters*, *412*, 152–162. https://doi.org/10.1016/j.epsl.2014.12.015

Engdahl, E. R., Di Giacomo, D., Sakarya, B., Gkarlaouni, C. G., Harris, J., & Storchak, D. A. (2020). ISC-EHB 1964-2016, an improved data set for studies of Earth structure and global seismicity. *Earth and Space Science*, *7*(1), e2019EA000897. https://doi.org/10.1029/2019ea000897

Fan, J. K., & Zhao, D. (2021). P-wave tomography and azimuthal anisotropy of the Manila-Taiwan-southern Ryukyu region. *Tectonics*, *40*(2), e2020TC006262. https://doi.org/10.1029/2020TC006262

Fan, J. K., Wu, S. G., & Spence, G. (2015). Tomographic evidence for a slab tear induced by fossil ridge subduction at Manila Trench, South China Sea. *International Geology Review*, *57*(5–8), 998–1013. https://doi.org/10.1080/00206814.2014.929054

Favier, N., & Chevrot, S. (2003). Sensitivity kernels for shear wave splitting in transverse isotropic media. *Geophysical Journal International*, *153*(1), 213–228. https://doi.org/10.1046/j.1365-246x.2003.01894.x

Fouch, M. J., & Fischer, K. M. (1998). Shear wave anisotropy in the Mariana subduction zone. *Geophysical Research Letters*, *25*(8), 1221–1224. https://doi.org/10.1029/98gl00650

Greve, S. M., Savage, M. K., & Hofmann, S. D. (2008). Strong variations in seismic anisotropy across the Hikurangi subduction zone, North Island, New Zealand. *Tectonophysics*, *462*(1–4), 7–21. https://doi.org/10.1016/j.tecto.2007.07.011

Guo, J., Zhao, L., Chen, X., Yang, Z., Li, H., & Liu, C. (2022). Theoretical modelling of seismic dispersion, attenuation and frequency-dependent anisotropy in a fluid-saturated porous rock with intersecting fractures. *Geophysical Journal International*, *230*(1), 580–606. https://doi.org/10.1093/gji/ggac070

Hammond, J. O. S., Wookey, J., Kaneshima, S., Inoue, H., Yamashina, T., & Harjadi, P. (2010). Systematic variation in anisotropy beneath the mantle wedge in the Java–Sumatra subduction system from shear-wave splitting. *Physics of the Earth and Planetary Interiors*, *178*(3–4), 189–201. https://doi.org/10.1016/j.pepi.2009.10.003

Hanna, J., & Long, M. D. (2012). SKS splitting beneath Alaska: Regional variability and implications for subduction processes at a slab edge. *Tectonophysics*, *530*, 272–285. https://doi.org/10.1016/j.tecto.2012.01.003

Harris, P. T., Macmillan-Lawler, M., Rupp, J., & Baker, E. K. (2014). Geomorphology of the oceans. *Marine Geology*, *352*, 4–24. https://doi.org/10.1016/j.margeo.2014.01.011

Hasegawa, A., & Sacks, I. S. (1981). Subduction of the Nazca plate beneath Peru as determined from seismic observations. *Journal of Geophysical Research*, *86*(B6), 4971–4980. https://doi.org/10.1029/JB086iB06p04971

Hayes, G. P., Moore, G. L., Portner, D. E., Hearne, M., Flamme, H., Furtney, M., & Smoczyk, G. M. (2018). Slab2, a comprehensive subduction zone geometry model. *Science*, *362*(6410), 58–61. https://doi.org/10.1126/science.aat4723

He, X., Tao, J., Cao, Y., Pan, F., He, E., Cao, L., & Zheng, Y. (2022). No seamount subduction, no magmatic arc? *Earth and Planetary Physics*, *6*(4), 424–429. https://doi.org/10.26464/epp2022031

He, X., & Zhou, Q. (2024). Explicit role of seamount subduction in upper plate deformation as exemplified in the Ryukyu subduction zone. *Journal of Asian Earth Sciences*, *276*, 106354. https://doi.org/10.1016/j.jseaes.2024.106354

Healy, D., Reddy, S. M., Timms, N. E., Gray, E. M., & Brovarone, A. V. (2009). Trench-parallel fast axes of seismic anisotropy due to fluid-filled cracks in subducting slabs. *Earth and Planetary Science Letters*, *283*(1–4), 75–86. https://doi.org/10.1016/j.epsl.2009.03.037

Huang, Y., Ide, S., Kato, A., Yoshida, K., Jiang, C., & Zhai, P. (2025). Fault material heterogeneity controls deep interplate earthquakes. *Science Advances*, *11*(9), eadr9353. https://doi.org/10.1126/sciadv.adr9353

Huang, Z., Zhao, D., & Wang, L. (2011). Frequency-dependent shear-wave splitting and multilayer anisotropy in northeast Japan. *Geophysical Research Letters*, *38*(8), L08302. https://doi.org/10.1029/2011GL046804

Iwamori, H. (2000). Thermal effects of ridge subduction and its implications for the origin of granitic batholith and paired metamorphic belts. *Earth and Planetary Science Letters*, *181*(1), 131–144. https://doi.org/10.1016/s0012-821x(00)00182-5

Jiang, H., Huang, H., He, E., Guo, J., & Qiu, X. (2025). Hydration in the crust and upper mantle near the extinct spreading ridge in the eastern subbasin, South China Sea. *Geophysical Research Letters*, *52*(16), e2025GL115670. https://doi.org/10.1029/2025gl115670

Jung, H., & Karato, S.-I. (2001). Water-induced fabric transitions in olivine. *Science*, *293*(5534), 1460–1463. https://doi.org/10.1126/science.1062235

Karato, S. I., Jung, H., Katayama, I., & Skemer, P. (2008). Geodynamic significance of seismic anisotropy of the upper mantle: New insights from laboratory studies. *Annual Review of Earth and Planetary Sciences*, *36*(1), 59–95. https://doi.org/10.1146/annurev.earth.36.031207.124120

Katayama, I., Jung, H., & Karato, S.-I. (2004). New type of olivine fabric from deformation experiments at modest water content and low stress. *Geology*, *32*(12), 1045–1048. https://doi.org/10.1130/g20805.1

Kong, F., Gao, S. S., Liu, K. H., Zhang, J., & Li, J. (2020). Seismic anisotropy and mantle flow in the Sumatra subduction zone constrained by shear wave splitting and receiver function analyses. *Geochemistry, Geophysics, Geosystems*, *21*(2), e2019GC008766. https://doi.org/10.1029/2019gc008766

Koulakov, I., Wu, Y. M., Huang, H. H., Dobretsov, N., Jakovlev, A., Zabelina, I., et al. (2014). Slab interactions in the Taiwan region based on the P-and S-velocity distributions in the upper mantle. *Journal of Asian Earth Sciences*, *79*, 53–64. https://doi.org/10.1016/j.jseaes.2013.09.026

Lallemand, S. E., Font, Y., Bijwaard, H., & Kao, H. (2001). New insights on 3-D plates interaction near Taiwan from tomography and tectonic implications. *Tectonophysics*, *335*(3–4), 229–253. https://doi.org/10.1016/s0040-1951(01)00071-3

Lallemand, S. E., Malavieille, J., & Calassou, S. (1992). Effects of oceanic ridge subduction on accretionary wedges: Experimental modeling and marine observations. *Tectonics*, *11*(6), 1301–1313. https://doi.org/10.1029/92tc00637

Laske, G., Masters, G., Ma, Z., & Pasyanos, M. (2013). Update on CRUST1. 0—A 1-degree global model of Earth's crust. *Geophysical Research Abstracts*, *15*(15), 2658.

Laske, G., Masters, G., Ma, Z., & Pasyanos, M. E. (2012). CRUST1.0: An updated global model of Earth's crust. *Geophysical Research Abstracts*, *14*(3), 743.

Leidig, M., & Zandt, G. (2003). Modeling of highly anisotropic crust and application to the Altiplano–Puna volcanic complex of the Central Andes. *Journal of Geophysical Research*, *108*(B1), 2014. https://doi.org/10.1029/2001JB000649
Li, J., Jin, X., Aiguo, R., Wu, S., Wu, Z., & Liu, J. (2004). Indentation tectonics in the accretionary wedge of middle Manila Trench. *Chinese Science Bulletin*, *49*(12), 1279–1288. https://doi.org/10.1360/03wd0412
Liu, K. H., Gao, S. S., Gao, Y., & Wu, J. (2008). Shear wave splitting and mantle flow associated with the deflected Pacific slab beneath northeast Asia. *Journal of Geophysical Research*, *113*(B1), B01305. https://doi.org/10.1029/2007JB005178
Long, M. D., & Silver, P. G. (2008). The subduction zone flow field from seismic anisotropy: A global view. *Science*, *319*(5861), 315–318. https://doi.org/10.1126/science.1150809
Long, M. D., & Silver, P. G. (2009). Shear wave splitting and mantle anisotropy: Measurements, interpretations, and new directions. *Surveys in Geophysics*, *30*(4), 407–461. https://doi.org/10.1007/s10712-009-9075-1
Long, M. D., & Wirth, E. A. (2013). Mantle flow in subduction systems: The mantle wedge flow field and implications for wedge processes. *Journal of Geophysical Research: Solid Earth*, *118*(2), 583–606. https://doi.org/10.1002/jgrb.50063
Lynner, C. (2021). Anisotropy-revealed change in hydration along the Alaska subduction zone. *Geology*, *49*(9), 1122–1125. https://doi.org/10.1130/g48860.1
Lynner, C., & Long, M. D. (2013). Sub-slab seismic anisotropy and mantle flow beneath the Caribbean and Scotia subduction zones: Effects of slab morphology and kinematics. *Earth and Planetary Science Letters*, *361*, 367–378. https://doi.org/10.1016/j.epsl.2012.11.007
Lynner, C., Toro-Acosta, C., Paulson, E., & Birkey, A. (2024). Local-S shear wave splitting along the length of the Alaska–Aleutian subduction zone. *Geophysical Journal International*, *237*(3), 1567–1574. https://doi.org/10.1093/gji/ggae107
Marson-Pidgeon, K., & Savage, M. K. (1997). Frequency-dependent anisotropy in Wellington, New Zealand. *Geophysical Research Letters*, *24*(24), 3297–3300. https://doi.org/10.1029/97gl03274
Marson-Pidgeon, K., & Savage, M. K. (2004). Shear-wave splitting variations across an array in the southern North Island, New Zealand. *Geophysical Research Letters*, *31*(21), L21602. https://doi.org/10.1029/2004gl021190
Nakajima, J. (2025). The Tokyo Bay earthquake nest, Japan: Implications for a subducted seamount. *Tectonophysics*, *906*, 230728. https://doi.org/10.1016/j.tecto.2025.230728
Pautot, G., & Rangin, C. (1989). Subduction of the South China Sea axial ridge below Luzon (Philippines). *Earth and Planetary Science Letters*, *92*(1), 57–69. https://doi.org/10.1016/0012-821x(89)90020-4
Rangin, C., Le Pichon, X., Mazzotti, S., Pubellier, M., Chamot-Rooke, N., Aurelio, M., et al. (1999). Plate convergence measured by GPS across the Sundaland/Philippine Sea plate deformed boundary: The Philippines and eastern Indonesia. *Geophysical Journal International*, *139*(2), 296–316. https://doi.org/10.1046/j.1365-246x.1999.00969.x
Russo, R. M., & Silver, P. G. (1994). Trench-parallel flow beneath the Nazca plate from seismic anisotropy. *Science*, *263*(5150), 1105–1111. https://doi.org/10.1126/science.263.5150.1105
Savage, M. K. (1999). Seismic anisotropy and mantle deformation: What have we learned from shear wave splitting? *Reviews of Geophysics*, *37*(1), 65–106. https://doi.org/10.1029/98rg02075
Savage, M. K., Wessel, A., Teanby, N., & Hurst, T. (2010). Automatic measurement of shear wave splitting and applications to time varying anisotropy at Mt. Ruapehu volcano, New Zealand. *Journal of Geophysical Research*, *115*, B12321. https://doi.org/10.1029/2010JB007722
Scholz, C. H., & Small, C. (1997). The effect of sea mount subduction on seismic coupling. *Geology*, *25*(6), 487–490. https://doi.org/10.1130/0091-7613(1997)025<0487:teosso>2.3.co;2
Silver, P. G., & Chan, W. W. (1991). Shear wave splitting and subcontinental mantle deformation. *Journal of Geophysical Research*, *96*(B10), 16429–16454. https://doi.org/10.1029/91jb00899
Silver, P. G., & Savage, M. K. (1994). The interpretation of shear-wave splitting parameters in the presence of two anisotropic layers. *Geophysical Journal International*, *119*(3), 949–963. https://doi.org/10.1111/j.1365-246x.1994.tb04027.x
Tan, H., Gao, X., Wang, K., Gao, J., & He, J. (2022). Hidden roughness of subducting seafloor and implications for megathrust seismogenesis: Example from northern Manila trench. *Geophysical Research Letters*, *49*(17), e2022GL100146. https://doi.org/10.1029/2022GL100146
Teanby, N., Kendall, J. M., & Van der Baan, M. (2004). Automation of shear-wave splitting measurements using cluster analysis. *Bulletin of the Seismological Society of America*, *94*(2), 453–463. https://doi.org/10.1785/0120030123
Tsai, Y. B., Liaw, Z. S., Lee, T. Q., Lin, M. T., & Yeh, Y. H. (1981). Seismological evidence of an active plate boundary in the Taiwan area. *Memoir of the Geological Society of China*, *4*, 143–154.
Volti, T., Kaneda, Y., Zatsepin, S., & Crampin, S. (2005). An anomalous spatial pattern of shear-wave splitting observed in ocean bottom seismic data above a subducting seamount in the Nankai trough. *Geophysical Journal International*, *163*(1), 252–264. https://doi.org/10.1111/j.1365-246x.2005.02743.x
Wang, J., Huang, X., Zhao, D., & Yao, Z. (2019). Seismic anisotropy evidence for ductile deformation of the forearc lithospheric mantle in subduction zones. *Journal of Geophysical Research: Solid Earth*, *124*(7), 7013–7027. https://doi.org/10.1029/2018jb016912
Wang, K., & Bilek, S. L. (2011). Do subducting seamounts generate or stop large earthquakes? *Geology*, *39*(9), 819–822. https://doi.org/10.1130/g31856.1
Wang, K., & Bilek, S. L. (2014). Invited review paper: Fault creep caused by subduction of rough seafloor relief. *Tectonophysics*, *610*, 1–24. https://doi.org/10.1016/j.tecto.2013.11.024
Wang, L., & He, X. (2020). Seismic anisotropy in the Java-Banda and Philippine subduction zones and its implications for the mantle flow system beneath the Sunda plate. *Geochemistry, Geophysics, Geosystems*, *21*(4), 1095. https://doi.org/10.1029/2019gc008658
Wang, Z., Zhao, D., Wang, J., & Kao, H. (2006). Tomographic evidence for the Eurasian lithosphere subducting beneath south Taiwan. *Geophysical Research Letters*, *33*(18), L18306. https://doi.org/10.1029/2006GL027166
Wessel, P., & Smith, W. H. (1991). Free software helps map and display data. *Eos, Transactions American Geophysical Union*, *72*(41), 441–446. https://doi.org/10.1029/90eo00319
Wirth, E. A., & Long, M. D. (2010). Frequency-dependent shear wave splitting beneath the Japan and Izu-Bonin subduction zones. *Physics of the Earth and Planetary Interiors*, *181*(3–4), 141–154. https://doi.org/10.1016/j.pepi.2010.05.006
Wirth, E. A., & Long, M. D. (2012). Multiple layers of seismic anisotropy and a low-velocity region in the mantle wedge beneath Japan: Evidence from teleseismic receiver functions. *Geochemistry, Geophysics, Geosystems*, *13*(8), Q08005. https://doi.org/10.1029/2012gc004180
Wu, W. N., Lo, C. L., & Lin, J. Y. (2017). Spatial variations of the crustal stress field in the Philippine region from inversion of earthquake focal mechanisms and their tectonic implications. *Journal of Asian Earth Sciences*, *142*, 109–118. https://doi.org/10.1016/j.jseaes.2017.01.036
Yang, T. F., Lee, T., Chen, C. H., Cheng, S. N., Knittel, U., Punongbayan, R. S., & Rasdas, A. R. (1996). A double island arc between Taiwan and Luzon: Consequence of ridge subduction. *Tectonophysics*, *258*(1–4), 85–101. https://doi.org/10.1016/0040-1951(95)00180-8
Yesson, C., Clark, M. R., Taylor, M. L., & Rogers, A. D. (2011). The global distribution of seamounts based on 30 arc seconds bathymetry data. *Deep-Sea Research Part I Oceanographic Research Papers*, *58*(4), 442–453. https://doi.org/10.1016/j.dsr.2011.02.004

Zhao, D., Yamamoto, Y., & Yanada, T. (2013). Global mantle heterogeneity and its influence on teleseismic regional tomography. *Gondwana Research*, *23*(2), 595–616. https://doi.org/10.1016/j.gr.2012.08.004

References From the Supporting Information

Pasyanos, M. E., Masters, G., Laske, G., & Ma, Z. (2014). LITHO1.0: An updated crust and lithospheric model of the Earth. *Journal of Geophysical Research: Solid Earth*, *119*(3), 2153–2173. https://doi.org/10.1002/2013jb010626